

## SUPPORTING INFORMATION

### **Kinetics and dynamics study of the $\text{OH} + \text{C}_2\text{H}_6 \rightarrow \text{H}_2\text{O} + \text{C}_2\text{H}_5$ reaction based on an analytical global potential energy surface**

C. Rangel, M. Garcia-Chamorro, J.C. Corchado and J. Espinosa-Garcia\*

Departamento de Química Física and Instituto de Computación Científica Avanzada,

Universidad de Extremadura

06071 Badajoz (Spain)

\* Corresponding authors: [joaquin@unex.es](mailto:joaquin@unex.es)

## Kinetics and dynamics computational details.

**1. Kinetics study.** Based on the PES-2020 surface previously developed, the rate constants were calculated using three approaches: variational transition-state theory with multidimensional tunnelling corrections (VTST/MT), ring polymer molecular dynamics (RPMD) and QCT calculations.

**a) VTST/MT approach.** The thermal rate constants at different temperatures in the range 200-2000 K were calculated using the canonical variational theory (CVT),<sup>1,2</sup>

$$k^{CVT}(T) = \sigma \frac{k_B T}{h} K^\circ \min_s \exp \left[ \frac{-\Delta G^{GT,\circ}(T, s^{*,CVT})}{k_B T} \right] \quad (S1)$$

where  $\sigma$ ,  $k_B$ ,  $T$ ,  $h$  and  $K^\circ$  are, respectively, the symmetry factor or number of equivalent paths, Boltzmann constant, temperature, Planck constant and reciprocal of the standard-state concentration, 1 molecule  $\text{cm}^3$ . In this theory, at each temperature, the dividing surface is varied,  $s^{*,CVT}$ , until the maximum of the free energy of activation,  $\Delta G$ , along the reaction coordinate,  $s$ . To estimate  $\Delta G$ , the rotational partition functions were calculated classically, while the vibrational partition functions were calculated as harmonic oscillators using redundant internal coordinates.<sup>3-5</sup> However, to treat the anharmonicity present in the lowest vibrational modes, the hindered rotor model (RW model)<sup>6</sup> was used. In addition, for the OH electronic partition function the  ${}^2\Pi_{1/2}$  excited state (excitation energy of  $\varepsilon = 140 \text{ cm}^{-1}$ )<sup>7</sup> was included. Therefore, the following electronic partition function ratio is used in Eq. S1,

$$f = \frac{2}{2 + 2 \exp(-\varepsilon / k_B T)} \quad (S2)$$

where the number 2 in the numerator corresponds to the transition state, in which the spin-orbit coupling is assumed to be fully quenched. Note that this multi-surface factor has an important role in the final rate constants, as it decreases the rate constant by a factor of about 2 at high temperatures. Finally, this reaction presents a heavy-light-heavy mass combination, which a priori is a good candidate to present tunneling at low temperatures, although given the low adiabatic barrier (when the zero-point energy, ZPE, is included in the classical barrier height) the tunneling factor will be small. The tunneling correction has been calculated by using the microcanonical optimized multidimensional tunnelling approach,  $\mu\text{OMT}$ .<sup>8</sup> The Polyrate-2016 code<sup>9</sup> was used in these kinetics calculations.

**b) RPMD approach.** A recent and useful alternative to the VTST approach is the ring polymer molecular dynamics approach.<sup>10-12</sup> The thermal rate constants are evaluated as the product of two factors,

$$k_{RPMD}(T) = k_{QTST}(T, \xi^{\ddagger}) \cdot \kappa(t \rightarrow \infty, \xi) \quad (\text{S3})$$

where  $k_{QTST}(T)$  represents the centroid-density quantum transition state theory rate constant at temperature  $T$  at the reaction coordinate  $\xi^{\ddagger}$ , which is evaluated from the potential of mean force (PMF) along  $\xi$  (Figure S1).  $\kappa(t \rightarrow \infty, \xi)$  represents the ring polymer transmission coefficient including recrossing effects (Figure S2). An advantage of the RPMD versus the VTST theory is that it is not affected by the location of the dividing surface between reactants and products, related with recrossing effects and associated with the harmonic/anharmonic description of the lowest vibrational frequencies. Given the very expensive computational cost, rate constants are limited to 298, 500, 1000, 1500 and 2000 K using the RPMD code.<sup>12</sup> Temperatures lower than 298 K were not calculated because it is known that the number of beads greatly increases at lower temperatures, and consequently the computational cost, which is beyond the limits of our current resources. Note that the electronic partition function is included using Eq. S2. Table S1 lists all parameters used in the present RPMD calculations.

**2. Dynamics study.** As noted previously in Introduction, the only experimental dynamics study was reported by Butkovskaya and Setser,<sup>13</sup> where the water product properties were analysed at 298 K for the  $\text{OH} + \text{C}_2\text{H}_6 \rightarrow \text{H}_2\text{O} + \text{C}_2\text{H}_5$  and the isotopic  $\text{OD} + \text{C}_2\text{H}_6 \rightarrow \text{HOD} + \text{C}_2\text{H}_5$  reactions. To simulate and explain these experimental findings, QCT calculations based on the PES-2020 surface were performed at 298 K using the VENUS code.<sup>14,15</sup> For each reaction,  $\text{H}_2\text{O}$  and  $\text{HOD}$  products, 1.5 million trajectories were run at this temperature with a propagation step of 0.1 fs, and to ensure reactant and product asymptotes with no interaction a C-O separation was fixed at 15.0 Å. The rotational and vibrational energies of reactants were selected by thermal sampling at this temperature, while the relative translational energy of the reactants was chosen from the following distribution,  $E(\text{RT})^2 \exp(-E/\text{RT})$ . The maximum impact parameter,  $b_{\text{max}} = 3.8$  Å, was obtained from successive and small batches of trajectories, until no reactive trajectories were found, while the remaining initial conditions (impact parameter, spatial orientation and vibrational phases) were selected from a Monte Carlo sampling. Knowing the number

of reactive ( $N_r$ ) and the total ( $N_T$ ) number of trajectories from the outcome of the QCT calculations, the reaction cross section at temperature  $T$  is defined as,

$$\sigma_r(T) = \pi b_{\max}^2 \frac{N_r}{N_T} \quad (\text{S4})$$

with a standard error of,

$$\Delta\sigma_r(T) = \sigma_r(T) \sqrt{\frac{N_T - N_r}{N_T \cdot N_r}} \quad (\text{S5})$$

which, in this case, presents a maximum error <5%, while the thermal rate constant is defined as,

$$k(T) = f \left( \frac{8k_B T}{\pi\mu} \right)^{1/2} \sigma_r(T) \quad (\text{S6})$$

where the multi-surface temperature factor  $f$  (Eq. S2) is included to take into account the fraction of reactant evolving on the ground-state surface. Note that for the sake of completeness and to compare QCT rate constants with values obtained using the VTST/MT and RPMD approaches, we also performed additional QCT calculations at 500, 1000, 1500 and 2000 K, where the same initial conditions were considered, changing the respective  $b_{\max}$  values: 4.7, 5.3, 5.1 and 5.0 Å, respectively, and the total number of trajectories run at each temperature, 500 000, because now only the number of reactive trajectories will be analysed and no more details are needed.

A known limitation in QCT calculations is the ZPE violation problem, i.e., how to treat trajectories that end with vibrational energy below its ZPE, and this problem affects all kinds of trajectories: reactive that evolves to products, H<sub>2</sub>O/HOD + C<sub>2</sub>H<sub>5</sub>, and non-reactive that returns to reactants, OH/OD and C<sub>2</sub>H<sub>6</sub>. We consider two approaches: i) all trajectories are considered independent of the ZPE (All-approach) and ii) we discard reactive trajectories where each product, H<sub>2</sub>O/HOD and C<sub>2</sub>H<sub>5</sub>, presents a vibrational energy below its ZPE, 12.96/11.2 and 36.31 kcal mol<sup>-1</sup>, respectively; in addition to this we discard non-reactive trajectories where each reactant, OH/OD and C<sub>2</sub>H<sub>6</sub>, appears with a vibrational energy below its ZPE, 5.40/4.02 and 46.05 kcal mol<sup>-1</sup>, respectively. This is a passive method<sup>16-20</sup> named DZPE (double ZPE approach). Another passive approach was proposed by Schatz et al.<sup>21,22</sup> where the ZPE correction is applied only to the new

H<sub>2</sub>O/HOD formed product (ZPE-H<sub>2</sub>O/HOD). However, for this reaction the ZPE – H<sub>2</sub>O/HOD and DZPE approaches give the same results.

Additionally, from the outcome of the standard QCT calculations at 298 K the following product dynamics properties were obtained: vibrational and rotational energies of the water and ethyl products, relative translational energy between products and scattering distribution. However, the water product vibrational actions were not directly obtained and they were calculated with the normal mode analysis method, implemented in the NMA code<sup>23</sup> (and obviously based on the same PES-2020 surface), which includes anharmonicity and Coriolis-coupling terms. These vibrational actions are denoted as H<sub>2</sub>O( $a_{\text{OH}}$ ,  $a_{\text{bending}}$ ,  $a_{\text{OH}^*}$ ) for the H<sub>2</sub>O product, associated with the symmetric OH stretch, 3700 cm<sup>-1</sup>, bending, 1580 cm<sup>-1</sup> and antisymmetric OH\* stretch, 3755 cm<sup>-1</sup>; and as HOD( $a_{\text{OD}}$ ,  $a_{\text{bending}}$ ,  $a_{\text{OH}}$ ) for the HOD product, associated with the OD stretch, 2718 cm<sup>-1</sup>, bending, 1382 cm<sup>-1</sup> and OH stretch, 3734 cm<sup>-1</sup>. Obviously, from quasi-classical calculations, these actions  $a_i$  are non-integer numbers, and they are rounded to the nearest integer value,  $n_i$ , to pseudo-quantize them. Finally, we deal the vibrational quantization using two binning approaches: i) standard or histogram binning (SB or HB) when all reactive trajectories contribute with weight unit, and ii) energy-based Gaussian binning (1GB),<sup>24,25</sup> where each trajectory is assigned Gaussian weight so that the larger weights correspond to product vibrational energies closer to their quantum values.

**Table S1.** Input parameters for the RPMD rate calculations on the OH + C<sub>2</sub>H<sub>6</sub> reaction.

The explanation of the format of the input file can be found in the RPMDrate code manual (see <http://rpmbrate.cyi.ac.cy/>)

Parameter	OH+C <sub>2</sub> H <sub>6</sub> --> H <sub>2</sub> O+C <sub>2</sub> H <sub>5</sub>	Explanation	
<b>Command line parameters</b>			
Temp.	298-2000	Temperature (K)	
$N_{\text{beads}}$	64 (298 K), 64 (500 K); 16 (1000 K), 4 (1500 K); 4 (2000 K)	Number of beads	
<b>Dividing Surface parameters</b>			
$R_{\infty}$	15	Dividing surface parameter (distance). Angstroms	
$N_{\text{bond}}$	1	Forming and breaking bonds	
$N_{\text{channel}}$	1	Equivalent product channels	
C	-1.31134307 0.32416192 0.43272614	Cartesian coordinates (x,y,z) of the intermediate geometry. (Angstroms)	
C	-1.53188503 0.37831214 1.91721022		
H	-0.24368511 0.26233974 0.21103467		
H	-1.80675435 -0.55091912 0.00722476		
H	-1.71478832 1.21998262 -0.04370759		
H	-1.15011358 -0.52394325 2.40943289		
H	-1.05707979 1.26278615 2.35807896		
H	-2.67932630 0.44450527 2.14100289		
O	-4.00429058 0.52108872 2.40317798		
H	-4.07334566 0.39587584 3.36359715		
Thermostat	'Andersen'		Thermostat option
<b>Biased sampling parameters</b>			
$N_{\text{windows}}$	110	Number of windows	
$\xi_i$	-0.05	Center of the first window	
$d\xi$	0.01	Window spacing step	
$\xi_N$	1.05	Center of the last window	
$dt$	0.0001	Time step (ps)	
$k_i$	2.72 1.36 (2000K)	Umbrella force constant ((T/K) eV)	
$N_{\text{trajectories}}$	100	Number of trajectories	
$t_{\text{equilibration}}$	20	Equilibration period (ps)	
$t_{\text{sampling}}$	100	Sampling period in each trajectory (ps)	
$N_i$	$2 \times 10^8$	Total number of sampling points	
<b>Potential mean force calculations</b>			
$\xi_0$	0.0	Start of umbrella integration	
$\xi_{\ddagger}$	298 (0.9777); 500 K (0.9908); 1000 K (1.0041); 1500 K (1.0107), 2000 K (0.9519)	End of umbrella integration	
$N_{\text{bins}}$	5000	Number of bins	
<b>Recrossing factor</b>			
$dt$	0.0001	Time step (ps)	
$t_{\text{equilibration}}$	20	Equilibration period (ps) in the constrained (parent) traj. (ps)	
$N_{\text{totalchild}}$	100000	Number of unconstrained (child) trajectories	
$t_{\text{childsampling}}$	2	Sampling increment along the parent trajectory (ps)	
$N_{\text{child}}$	100	Number of child trajectories per one initially constrained configuration	
$t_{\text{child}}$	0.05	Length of child trajectories (ps)	

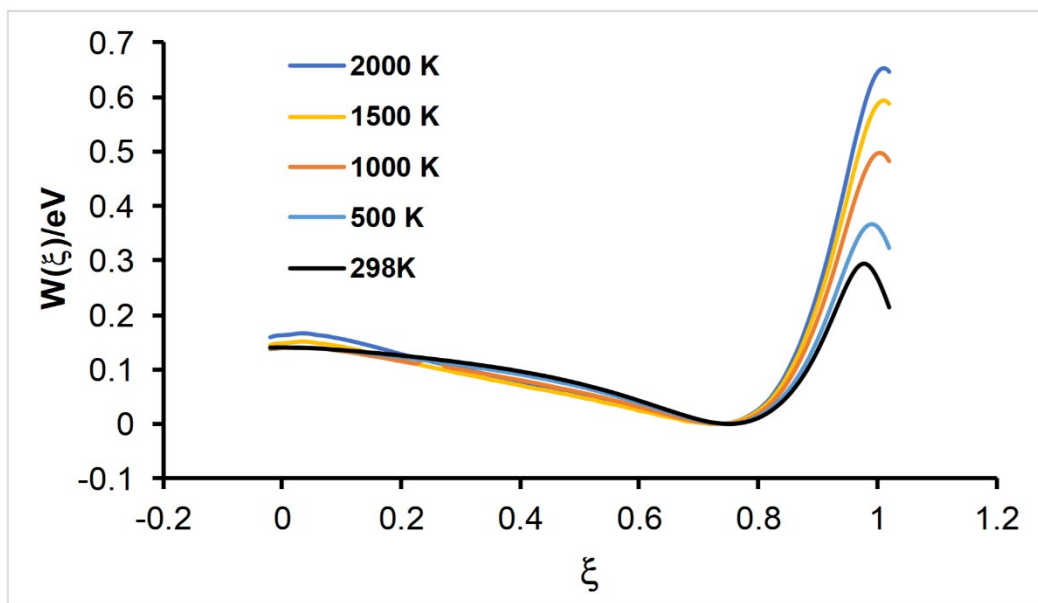


**Figure S1.** Ring polymer potentials of mean force (free energy) at 298-2000 K for the  $\text{OH} + \text{C}_2\text{H}_6$  reaction.

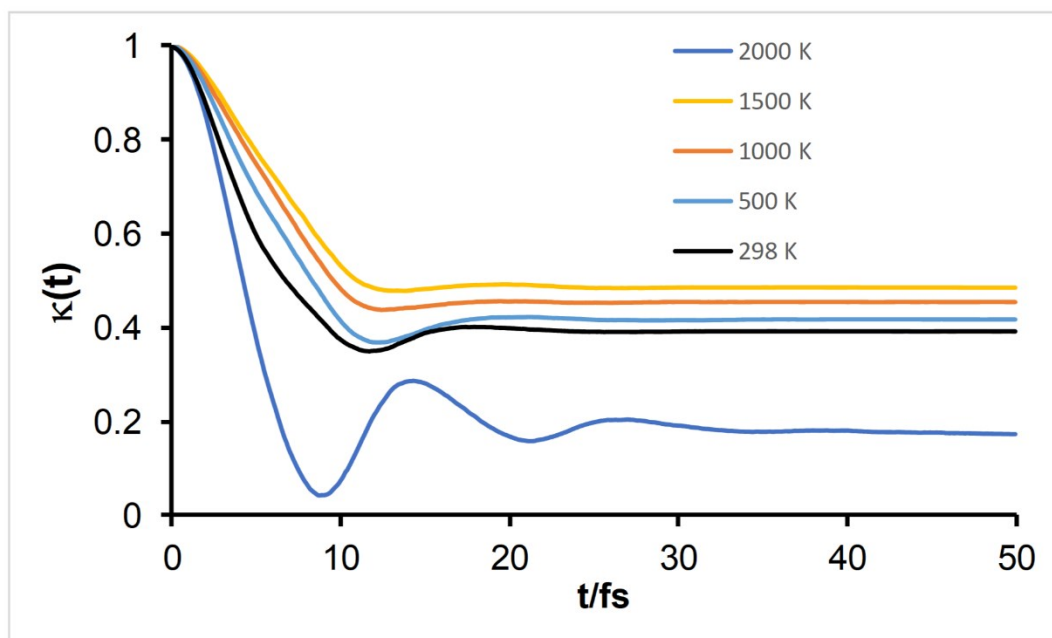


**Figure S2.** Ring polymer transmission coefficients at 298-2000 K for the  $\text{OH} + \text{C}_2\text{H}_6$  reaction.

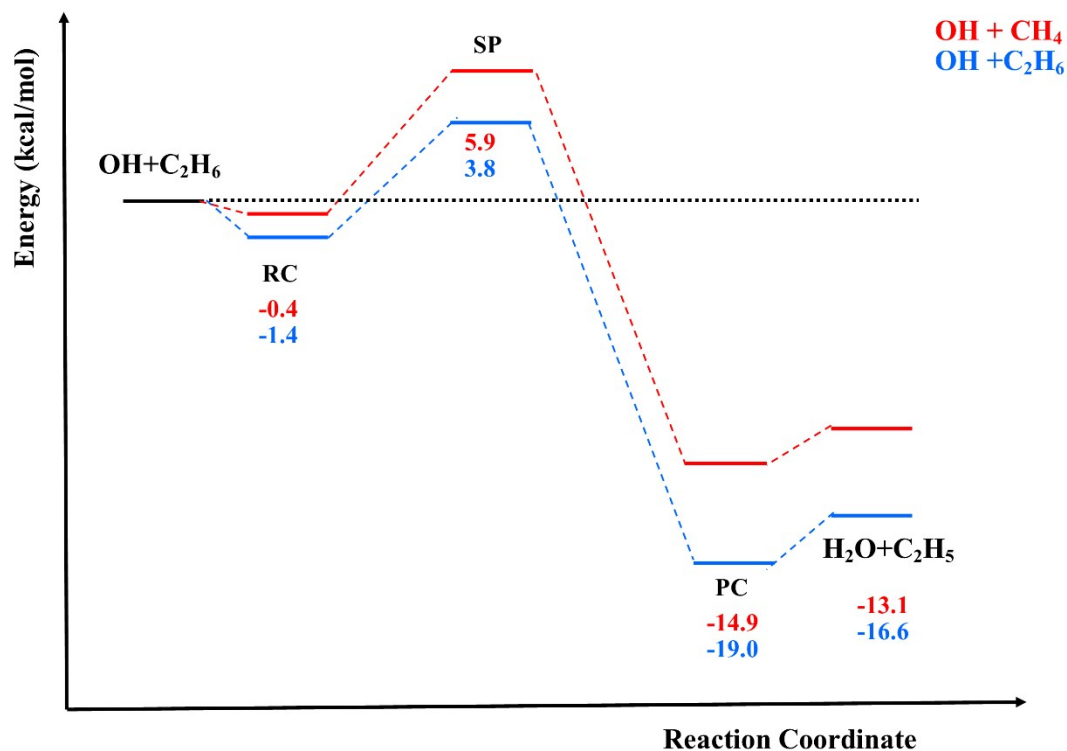


**Figure S3.** Schematic energy profiles of the stationary points for the OH + C<sub>2</sub>H<sub>6</sub> (at the Level 1: CCSD(T)-F12a/aug-cc-pVTZ//CCSD(T)/cc-pVTZ) and OH + CH<sub>4</sub> (PMP2 level based on the extrapolation of energies obtained by using correlation-consistent polarized double and triple-zeta basis sets, cc-pVDZ and cc-pVTZ, from Ref. 26) reactions. RC, SP and PC mean, respectively, reactant complex, saddle point and product complex.

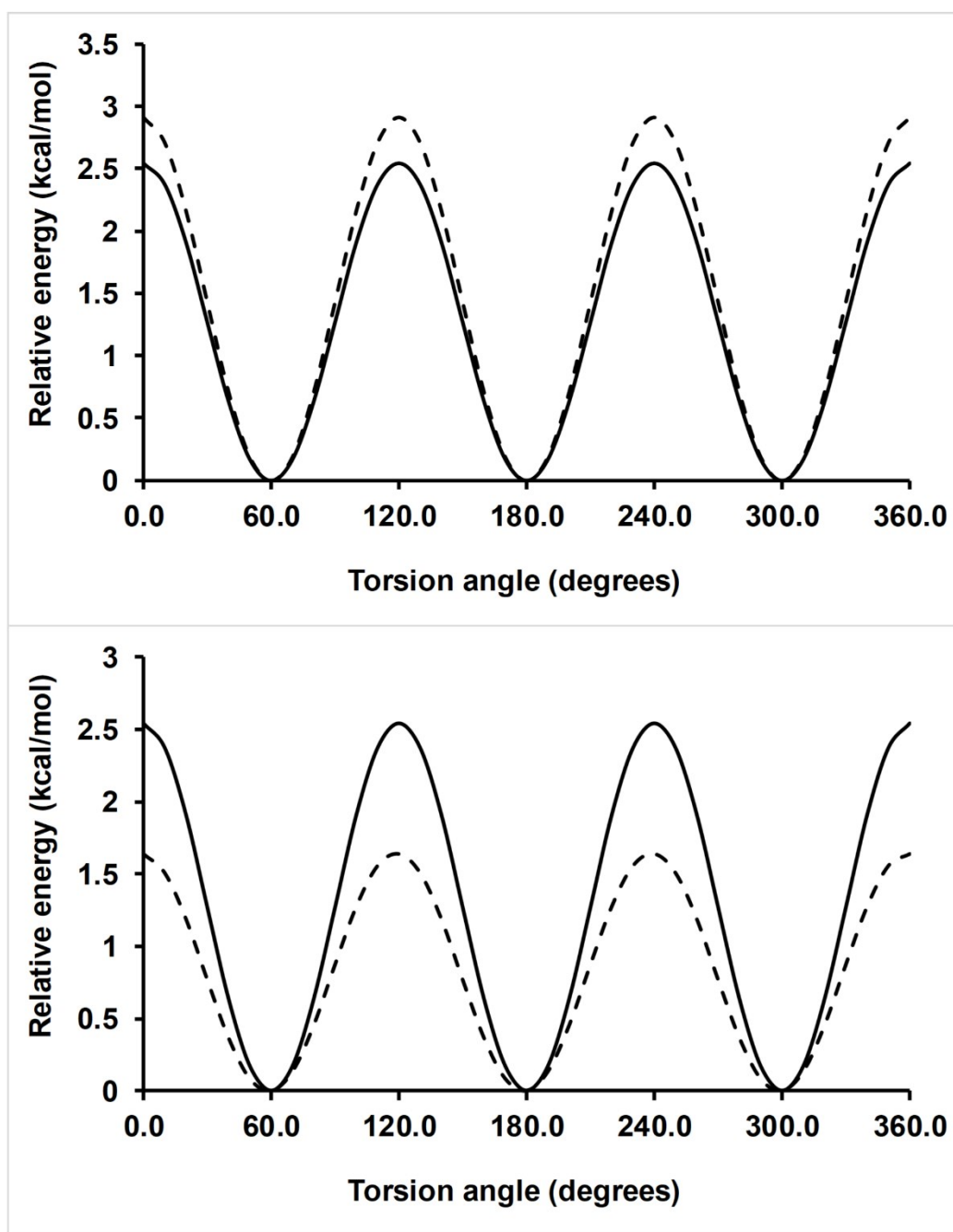


**Figure S4:** Upper panel: ethane torsional barrier, in kcal mol<sup>-1</sup>, using PES-2020 (solid line) and the CCSD(T)/cc-pVTZ level (dashed line). Lower panel: Ethane (solid line) and saddle point (dashed line) torsional barriers using PES-2020 (in kcal mol<sup>-1</sup>). Note that these plots correspond to frozen scans, where only the torsional angle is varied. The remain fixed coordinates correspond to the optimized geometries at the stationary point at each level.

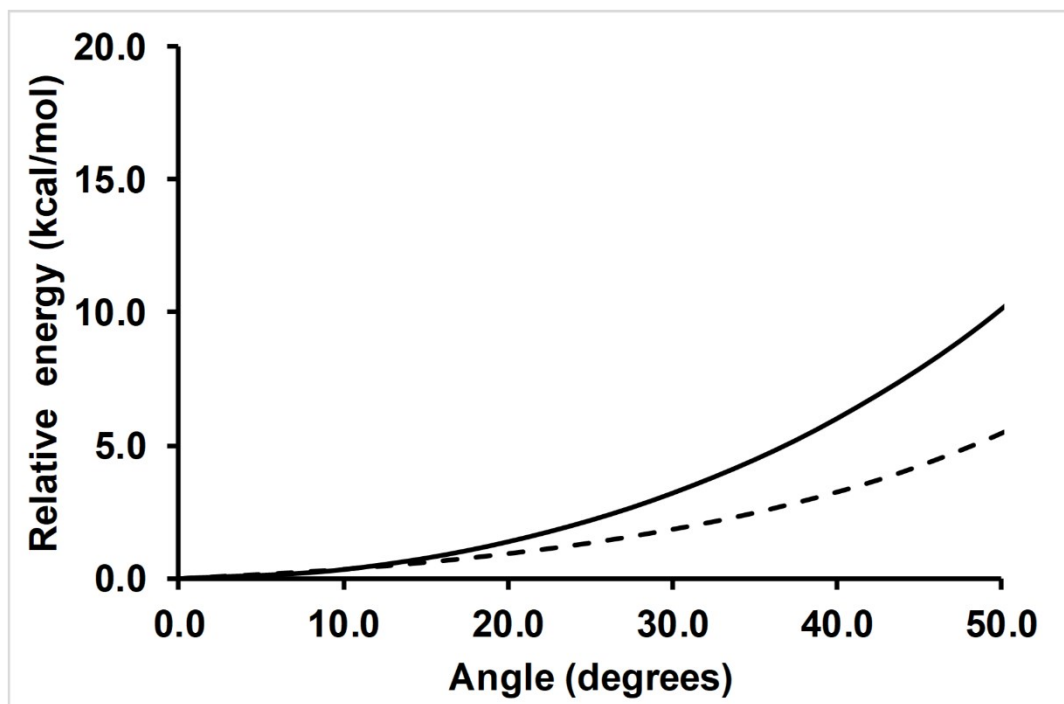


**Figure S5:** Energy dependence on the C-H'-O bonding angle in the saddle point, in kcal mol<sup>-1</sup>. Solid line, PES-2020 and dashed line, CCSD(T)/cc-pVTZ level. In both curves, the respective equilibrium angle at the saddle point is taken as level zero and the remaining geometric parameters are kept fixed at the respective saddle point geometry. In both curves, the C-C-H'-O dihedral angle is fixed at 180°.

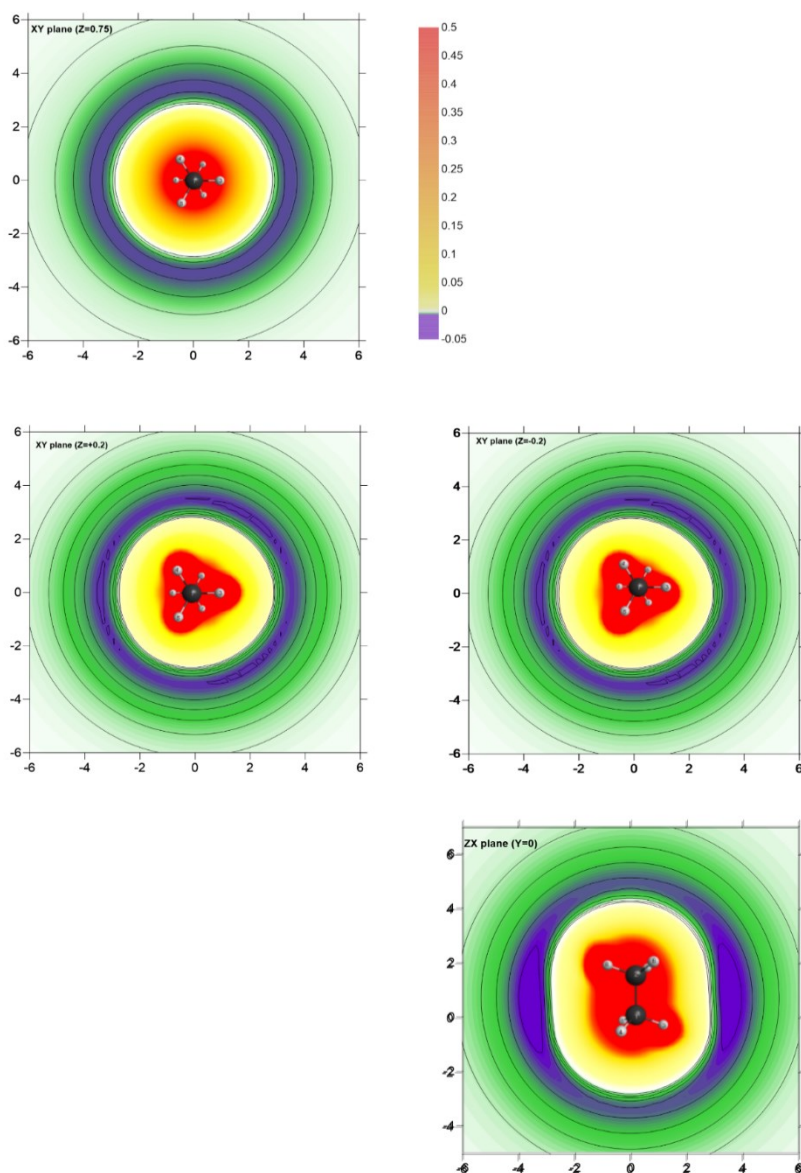


**Figure S6:** Contour plots of the PES-2020 potential created by ethane in its equilibrium bond length. The energy scale refers to  $\text{C}_2\text{H}_6 + \text{OH}$  asymptotic limit energy. Yellow to red contours indicate positive energies, green to purple show negative values and white corresponds to zero energy with respect to the asymptotic limit. The upper panels show the energy in a plane perpendicular to the C-C bond and located in the central point of this bond. The middle panels present planes containing the three hydrogen atoms bonded to each carbon. The lower panel shows the energy in the plane containing the C-C bond and one of the three  $C_2$  symmetry axes of the ethane molecule. The C-C bond is placed on the Z axis, with one C fixed at  $Z=0$ . Distances in X and Y axis are given in Å and potential energy is given in  $\text{kcal mol}^{-1}$ .

**Table S2.** Activation energies (kcal mol<sup>-1</sup>) for the OH + C<sub>2</sub>H<sub>6</sub> reaction at different temperatures using CVT/ $\mu$ OMT on PES-2020.

T(K)	210- 300	298- 300	300- 400	495- 505	500- 600	595- 605	1000- 1500	2000- 2500
This work	1.72	2.11	2.39	3.24	3.48	3.76	5.23	12.07
CVT/SCT <sup>a</sup>	2.04	1.44	1.69	2.76	3.07	3.42	7.24	12.26
Exp <sup>b</sup>	2.21	2.11	2.26	2.91	3.09	3.30		

a) Theoretical calculations from Ref. 27

b) Experimental values from Refs. 28,29.

**Table S3.** Thermal rate constant ratio at 298 K for the OH + C<sub>2</sub>H<sub>6</sub>/CH<sub>4</sub> reactions.

Reference	Ratio
CVT <sup>a</sup>	49.50
RPMD <sup>a</sup>	72.03
Exp <sup>b</sup>	35.87

a) PES-2020 and PES-2015 for OH + C<sub>2</sub>H<sub>6</sub> and OH + CH<sub>4</sub>, respectively. OH + CH<sub>4</sub>/PES-2015 from Ref. 30.

b) Experimental values from NIST kinetics Database (Ref. 31)

## References

1. B. C. Garrett and D. G. Truhlar, *J. Am. Chem. Soc.* 1979, 101, 4534.
2. D. G. Truhlar, A. D. Isaacson and B. C. Garrett, Generalized Transition State Theory. In *Theory of Chemical Reaction Dynamics*; Baer, M., Ed.; CRC Press: Boca Raton, FL, 1985; Vol. 4, pp 65–137.
3. C.F. Jackels, Z. Gu and D.G. Truhlar, *J. Chem. Phys.*, 1995, 102, 3188.
4. G.A. Natanson, B.C. Garrett, T.N. Truong, T. Joseph and D.G. Truhlar, *J. Chem. Phys.* 1991, 94, 7875.
5. Y.Y. Chuang and D.G. Truhlar, *J. Phys. Chem. A* 1997, 101, 3808.
6. D.G. Truhlar, *J. Comput. Chem.* 1991, 12, 266.
7. JANAF *Thermochemical Tables*, 3rd ed., edited by M. W. Chase, Jr., C. A. Davies, J. R. Downey, D. J. Frurip, R. A. McDonald, and A. N. Syverud, National Bureau of Standards, Washington, D.C., 1985, Vol. 14.
8. Y-P. Liu, D. h. Lu, A. Gonzalez-Lafont, D. G. Truhlar and B. C. Garrett, *J. Am. Chem. Soc.* 1993, 115, 7806.
9. J. Zheng, J.L. Bao, R. Meana-Paneda, S. Zhang, B.J. Lynch, J.C. Corchado, Y.Y. Chuang, P.L. Fast, W.P. Hu, Y.P. Liu, G.C. Lynch, K.A. Nguyen, C.F. Jackles, A. Fernandez-Ramos, B.A. Ellingson, V.S. Melissas, J. Villa, I. Rossi, E.L. Coitiño, J. Pu, T.V. Albu, A. Ratkiewicz, R. Steckler, B. C. Garret, A.D. Isaacson and D.G. Truhlar, POLYRATE-2016-2A, University of Minnesota, Minneapolis, MN, 2016.
10. R. Colleparado-Guevara, Y.V. Suleimanov and D.E Manolopoulos, *J. Chem. Phys.* 2009, 130, 174713; *ibid* 2010, 133, 049902.
11. Y.V. Suleimanov, R. Colleparado-Guevara and D.E. Manolopoulos, *J. Chem. Phys.* 2011, 134, 044131.
12. Y.V. Suleimanov, J.W. Allen and W.H. Green, *Comp. Phys. Comm.* 2013, 184, 833.
13. N.I. Butkovskaya and D.W. Setser, *Int. Rev. Phys. Chem.* 2003, 22, 1.
14. X. Hu, W.L. Hase and T. Pirraglia, *J. Comput. Chem.* 1991, 12, 1014.
15. W.L. Hase, R.J. Duchovic, X. Hu, A. Komornicki, K.F. Lim, D-h. Lu, G.H. Peslherbe, K.N. Swamy, S.R. Vande Linde, A.J.C. Varandas, H. Wang and R.J. Wolf, VENUS96: A General Chemical Dynamics Computer Program, *QCPE Bull.* 1996, 16, 43.
16. G. Nyman and J. Davidsson, *J. Chem. Phys.* 1990, 92, 2415.

17. A.J.C. Varandas and J.M.C. Marques, *J. Chem. Phys.* 1992, 97, 4050.
18. A.J.C. Varandas, *J. Chem. Phys.* 1993, 99, 1076.
19. G. Nyman, *Chem. Phys.* 1993, 173, 159.
20. A.J.C. Varandas, *Chem. Phys.Lett.* 1994, 225, 18.
21. K. Kudla and G. C. Schatz. *Chem. Phys.* 1993, 175, 71.
22. G. A. Bethardy, A. F. Wagner, G. C. Schatz and M. A. ter Horst. *J. Chem. Phys.* 1997, 106, 6001.
23. J.C. Corchado and J. Espinosa-Garcia, *Phys. Chem. Chem. Phys.* 2009, 11, 10157.
24. G. Czako and J.M. Bowman, *J. Chem. Phys.* 2009, 131, 244302.
25. L. Bonnet and J. Espinosa-Garcia, *J. Chem. Phys.* 2010, 133, 164108.
26. J. Espinosa-Garcia and J.C. Corchado, *Theor.Chem.Acc.* 2015, **134**, 6.
27. V.S. Melissas and D.G. Truhlar, *J. Phys.Chem.*, 1994, 98, 875.
28. R.J. Atkinson, *Phys. Chem. Ref. Data*, 1989, Monograph 1, 18.
29. R.K. Talukdar, A. Mellouki, T. Gierczak, S. Barone, S-Y. Chiang and A.R. Ravishankara, In 1991 Fall Meeting, American Geophysical Union: San Francisco, CA, 1991; p 101.
30. Y.V. Suleymanov and J. Espinosa-Garcia, *J.Phys.Chem. B* 2016, **120**, 1418.
31. NIST Chemical Kinetics Database web page. Standard References Database 17, Version 7.0 (Web Version), Release 1.6.8. Data Version 2015.9